Structural Engineering and Mechanics, Vol. 38, No. 6 (2011) 753-765
DOI: http://dx.doi.org/10.12989/sem.2011.38.6.753

Radial vibration behaviors of cylindrical composite piezoelectric transducers integrated with functionally graded elastic layer

H.M. Wang*, Y.K. Wei and Z.X. Xu

Department of Mechanics, Zhejiang University, Hangzhou 310027, P. R. China

(Received May 24, 2010, Accepted February 22, 2011)

Abstract. The radial vibration behaviors of a circular cylindrical composite piezoelectric transducer (CPT) are investigated. The CPT is composed of a piezoelectric ring polarized in the radial direction and an elastic ring graded in power-law variation form along the radial direction. The governing equations for plane stress state problem under the harmonic excitation are derived and the exact solutions for both piezoelectric and functionally graded elastic rings are obtained. The characteristic equations for resonant and anti-resonant frequencies are established. The presented methodology is fit to carry out the parametric investigation for composite piezoelectric transducers (CPTs) with arbitrary thickness in radial direction. With the aid of numerical analysis, the relationship between the radial vibration behaviors of the cylindrical CPT and the material inhomogeneity index of the functionally graded elastic ring as well as the geometric parameters of the CPTs are illustrated and some important features are reported.

Keywords: composite piezoelectric transducer; electromechanical coupling; cylindrical structure; radial vibration; functionally graded material

1. Introduction

The electro-mechanical coupling effect makes the piezoelectric materials widely used in various devices and systems. For the direct piezoelectric effect, the piezoelectric materials convert the mechanical forces into electrical signals (piezoelectric sensors) or electrical energy (energy harvesters). While for the inverse piezoelectric effect, the piezoelectric materials convert the electrical energy into mechanical motion (piezoelectric actuators) or vibrations (ultrasonic motors). Both the direct and inverse piezoelectric effects open up a wide range of applications in modern industry and engineering (Irschik 2002, Yang 2006, 2007, Leinvuo *et al*. 2007, Rao and Narayanan 2007, Jiang and Hu 2007, Mo *et al*. 2010).

In most smart devices and systems, the active element is a piezoelectric ceramic. For different purposes, the active element can be designed in various configurations (plates, tubes, spheres, rings or shells etc.). It is well known that when the piezoelectric element driven by different electrical or mechanical excitations, even for the same shape and same boundary conditions, the electrical and mechanical behaviors will be totally different. So it is always imperative to know the electrical and

*Corresponding author, Ph.D., E-mail: wanghuiming@zju.edu.cn

mechanical behaviors of the piezoelectric active element deeply in designing the effective intelligent structures.

Cylindrical structures are common components in various intelligent equipments. In the last decades, many substantial investigations in relation to cylindrical piezoelectric structures have been reported in different point of view. Bugdayci *et al.* (1983) studied the axisymmetric low frequency responses of radially polarized piezoelectric cylinders used in ink jet printing technology. Adelman *et al.* (1975) studied the axisymmetric vibrations of radially polarized piezoelectric cylinders subjected to different boundary conditions. Kim and Lee (2007) investigated the dynamic characteristics of piezoelectric cylindrical transducers with radial polarization. The steady state electro-mechanical responses of a long piezoelectric tube subjected to dynamic loading was solved by Huang *et al.* (2008). The investigations of transient responses in piezoelectric hollow cylinder excited by the dynamic electrical and mechanical loads were carried out by Ding *et al.* (2003). Wang *et al.* (2009) obtained the exact solution of a finite piezoelectric hollow cylinder under the torsional excitation. Elmaimouni *et al.* (2011) investigated the frequency spectrum of a cylindrically anisotropic piezoelectric disc resonator by using a mapped orthogonal functions technique.

To improve the electrical and mechanical behaviors (strength, stiffness, stability, radiating efficiency, electro-mechanical coupling factor) of the piezoelectric devices, an efficient way is combined the piezoelectric active elements with the proper elastic layers. Liu and Lin (2009) derived the radial electro-mechanical equivalent circuit of a composite piezoelectric transducer composed of a piezoelectric circular ring and a metal circular ring and then they analyzed the radial vibration behavior of the CPT. In the under water sound engineering, this kind of integrated transducers are benefit to increase their power capacity and stiffness. Lü *et al.* (2009) investigated the power transmission through a CPT, which is sandwiched by two piezoelectric layers and an elastic layer in the middle. By using the functionally graded materials, the electrical and mechanical behaviors of the piezoelectric transducers can also be improved. Alibeigloo (2009) studied the static responses of a functionally graded cylindrical shell with piezoelectric layers act as sensors and actuators. In this analysis, the material properties of the piezoelectric layer are constant and the Young's modulus of the elastic layer varies as an exponential function along the radial direction. Zhang *et al.* (2008) investigated the vibration characteristics of a functionally graded piezoelectric cylindrical actuator. They assume the actuator is polarized in the radial direction and the piezoelectric coefficient d_{31} varying linearly along the axial direction. Yu and Ma (2008) studied the circumferential wave in functionally graded piezoelectric cylindrical curved plates. Yu *et al*. (2009) studied the wave characteristics in functionally graded piezoelectric hollow cylinders.

Despite the variety of success, the investigation of the electrical and mechanical behaviors for the CPTs integrated with a functionally graded elastic layer still remains incomplete. This paper is aim to pursue a fundamental understanding of the electrical and mechanical behaviors of such kind of CPTs. The radial vibration characteristics of the CPTs were analyzed quantitatively by using the elasticity and piezoelectricity theories. The elastic layer is assumed to be graded in a power-law variation form along the radial direction. By setting the material inhomogeneity index equal to zero, this inhomogeneous model can be degenerated into the homogeneous one. Thus, the solution of the CPTs integrated with homogeneous elastic layers is fully covered by the presented solution. Numerical results produced by the present solution show good agreement with the having reported theoretical results and experimental data. Further parametric investigations for the CPTs integrated with functionally graded (FG) elastic layer are illustrated graphically.

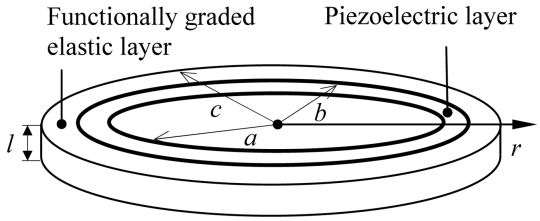

Fig. 1 Schematic of a cylindrical composite piezoelectric transducer

2. Governing equations and solutions of the CPT

Fig. 1 shows the schematic of a cylindrical composite piezoelectric transducer consisting of two rings. The inner part is piezoelectric and the outer is elastic. The innermost and outermost radii are a and c, respectively and the radius of the interface is b. The height of the CPT is l and the piezoelectric ring is polarized in the radial direction.

2.1 Solution for homogeneous piezoelectric ring

The ring type transducers have been widely used in underwater sound and ultrasonic technology and quite a number of literatures can be cited (Yang 2007, Liu and Lin 2009, Ramesh and Ebenezer 2005). For ring type transducer, the outer radius of the transducers is much larger than the height ($l \ll c$) and the upper and bottom surfaces are free from tractions. So it is reasonable to employ the plane stress state assumption to analyze this problem. Furthermore, in underwater sound and ultrasonic technology, the radial vibration mode has more practical applications and has been concerned widely (Liu and Lin 2009, Lü *et al*. 2009, Shin *et al*. 2003). Considering the practical usage, here we focus the investigation on the radial vibration of CPTs.

In the cylindrical coordinate system (r, θ, z), for radial vibration, all the field variables are only the functions of radial position r and the time variable t. For harmonic motion, all the fields have the same time dependent factor $\exp(\mathbf{j}\omega t)$ (Chen *et al*. 2004, Kim and Lee 2007). Here we dropped it for brevity. The notation ω is the angular frequency and $\mathbf{j}$ is the imaginary unit. Then for plane stress case, the equations of motion for piezoelectric ring can be simplified as

$$\frac{d\sigma_{rr}}{dr} + \frac{\sigma_{rr} - \sigma_{\theta\theta}}{r} + \rho\omega^2 u_r = 0 \tag{1a}$$

$$\frac{dD_r}{dr} + \frac{D_r}{r} = 0 \tag{1b}$$

where ρ is the mass density, u_r is the radial component of the mechanical displacement, σ_{rr} and $\sigma_{\theta\theta}$ are the radial and hoop stresses, D_r is the radial electric displacement. For radially polarized piezoelectric media with the crystal class 2 mm, the constitutive relations can be simplified as (Nye 1985, Ding and Chen 2001)

$$\begin{aligned}
\sigma_{\theta\theta} &= c_{11}\varepsilon_{\theta\theta} + c_{12}\varepsilon_{zz} + c_{13}\varepsilon_{rr} - e_{31}E_r \\
\sigma_{zz} &= c_{12}\varepsilon_{\theta\theta} + c_{22}\varepsilon_{zz} + c_{23}\varepsilon_{rr} - e_{32}E_r \\
\sigma_{rr} &= c_{13}\varepsilon_{\theta\theta} + c_{23}\varepsilon_{zz} + c_{33}\varepsilon_{rr} - e_{33}E_r
\end{aligned} \tag{2a}$$

$$D_r = e_{31}\varepsilon_{\theta\theta} + e_{32}\varepsilon_{zz} + e_{33}\varepsilon_{rr} + \in_{33} E_r \tag{2b}$$

where $\varepsilon_{ii}(i = r, \theta, z)$, E_r and Φ are the strain, electric field and electric potential, respectively. c_{ij}, e_{3i} and $\in_{33}$ are the elastic, piezoelectric and dielectric constants, respectively. The generalized geometric equations can be simplified as

$$\varepsilon_{rr} = \frac{du_r}{dr}, \quad \varepsilon_{\theta\theta} = \frac{u_r}{r} \tag{3a}$$

$$E_r = -\frac{d\Phi}{dr} \tag{3b}$$

Utilizing the plane stress condition $\sigma_{zz} = 0$, we obtained the following equation from the second equation of Eq. (2a).

$$\varepsilon_{zz} = \frac{1}{c_{22}}[-(c_{12}\varepsilon_{\theta\theta} + c_{23}\varepsilon_{rr}) + e_{32}E_r] \tag{4}$$

Substituting Eq. (4) into the expressions of $\sigma_{\theta\theta}, \sigma_{rr}$ and D_r in Eqs. (2a,b), we obtain

$$\begin{aligned} \sigma_{\theta\theta} &= \tilde{c}_{11}\frac{u_r}{r} + \tilde{c}_{13}\frac{du_r}{dr} + \tilde{e}_{31}\frac{d\Phi}{dr} \\ \sigma_{rr} &= \tilde{c}_{13}\frac{u_r}{r} + \tilde{c}_{33}\frac{du_r}{dr} + \tilde{e}_{33}\frac{d\Phi}{dr} \end{aligned} \tag{5a}$$

$$D_r = \tilde{e}_{31}\frac{u_r}{r} + \tilde{e}_{33}\frac{du_r}{dr} - \tilde{\in}_{33}\frac{d\Phi}{dr} \tag{5b}$$

where

$$\begin{aligned} &\tilde{c}_{11} = c_{11} - \frac{c_{12}^2}{c_{22}}, \quad \tilde{c}_{13} = c_{13} - \frac{c_{12}}{c_{22}}c_{23}, \quad \tilde{c}_{33} = c_{33} - \frac{c_{23}^2}{c_{22}} \\ &\tilde{e}_{31} = e_{31} - \frac{c_{12}}{c_{22}}e_{32}, \quad \tilde{e}_{33} = e_{33} - \frac{c_{23}}{c_{22}}e_{32}, \quad \tilde{\in}_{33} = \in_{33} + \frac{e_{32}^2}{c_{22}} \end{aligned} \tag{6}$$

The solution of Eq. (1b) takes the form as

$$D_r = A_1 r^{-1} \tag{7}$$

where A_1 is a unknown constant. Subsequently, Eq. (5b) can be rewritten as

$$\frac{d\Phi}{dr} = \frac{1}{\tilde{\in}_{33}}\left(\tilde{e}_{31}\frac{u_r}{r} + \tilde{e}_{33}\frac{du_r}{dr} - \frac{A_1}{r}\right) \tag{8}$$

With the aid of Eq. (8), Eq. (5a) becomes

$$\begin{aligned} \sigma_{\theta\theta} &= \bar{c}_{11}\frac{u_r}{r} + \bar{c}_{13}\frac{du_r}{dr} - \bar{e}_{31}\frac{A_1}{r} \\ \sigma_{rr} &= \bar{c}_{13}\frac{u_r}{r} + \bar{c}_{33}\frac{du_r}{dr} - \bar{e}_{33}\frac{A_1}{r} \end{aligned} \tag{9}$$

where

$$\bar{c}_{11} = \tilde{c}_{11} + \tilde{e}_{31}\bar{e}_{31}, \quad \bar{c}_{13} = \tilde{c}_{13} + \tilde{e}_{33}\bar{e}_{31}, \quad \bar{c}_{33} = \tilde{c}_{33} + \tilde{e}_{33}\bar{e}_{33}$$
$$\bar{e}_{31} = \tilde{e}_{31}/\tilde{\in}_{33}, \quad \bar{e}_{33} = \tilde{e}_{33}/\tilde{\in}_{33} \tag{10}$$

The substitution of Eq. (9) into Eq. (1a) derives

$$r^2\frac{d^2u_r}{dr^2} + r\frac{du_r}{dr} + [(k_p r)^2 - \mu_p^2]u_r = A_1 G \tag{11}$$

where

$$k_p = \frac{\omega}{c_p}, \quad c_p = \sqrt{\frac{\bar{c}_{33}}{\rho}}, \quad \mu_p = \sqrt{\frac{\bar{c}_{11}}{\bar{c}_{33}}}, \quad G = -\frac{\bar{e}_{31}}{\bar{c}_{33}} \tag{12}$$

The solution of Eq. (11) is

$$u_r(k_p, r) = A_1 H(k_p r) + A_2 J_{\mu_p}(k_p r) + A_3 Y_{\mu_p}(k_p r) \tag{13}$$

where $J_{\mu_p}(\cdot)$ and $Y_{\mu_p}(\cdot)$ are Bessel functions of the first and second kinds of order μ_p and $H(k_p r)$ is the particular solution of Eq. (11) which can be expressed by Lommel function as (Erdelyi 1953, Lü *et al*. 2009)

$$H(k_p r) = GS_{-1,\mu_p}(k_p r) \tag{14}$$

Essentially, $S_{-1,\mu_p}(k_p r)$ can be expressed by the Bessel functions as

$$S_{-1,\mu_p}(k_p r) = \frac{\pi}{2}[Y_{\mu_p}(k_p r)\int_a^r r^{-1}J_{\mu_p}(k_p r)dr - J_{\mu_p}(k_p r)\int_a^r r^{-1}Y_{\mu_p}(k_p r)dr] \tag{15}$$

Integrating Eq. (8) at the spatial interval $[a, r]$ and utilizing Eq. (13), we obtain

$$\Phi(k_p, r) = A_1\Phi_1(k_p, r) + A_2\Phi_2(k_p, r) + A_3\Phi_3(k_p, r) + \Phi_a \tag{16}$$

where Φ_a is the electric potential at the internal surface of the piezoelectric ring and

$$\Phi_1(k_p, r) = \bar{e}_{33}[H(k_p r) - H(k_p a)] + \bar{e}_{31}\int_a^r r^{-1}H(k_p r)dr - \frac{1}{\tilde{\in}_{33}}\ln\left(\frac{r}{a}\right)$$
$$\Phi_2(k_p, r) = \bar{e}_{33}[J_{\mu_p}(k_p r) - J_{\mu_p}(k_p a)] + \bar{e}_{31}\int_a^r r^{-1}J_{\mu_p}(k_p r)dr$$
$$\Phi_3(k_p, r) = \bar{e}_{33}[Y_{\mu_p}(k_p r) - Y_{\mu_p}(k_p a)] + \bar{e}_{31}\int_a^r r^{-1}Y_{\mu_p}(k_p r)dr \tag{17}$$

Substituting Eq. (13) into the second equation in Eq. (9), gives

$$\sigma_{rr}(k_p, r) = A_1\sigma_{p1}(k_p, r) + A_2\sigma_{p2}(k_p, r) + A_3\sigma_{p3}(k_p, r) \tag{18}$$

where

$$\sigma_{p1}(k_p, r) = \Re_p[H(k_p r)] - \bar{e}_{33} r^{-1}, \quad \sigma_{p2}(k_p, r) = \Re_p[J_{\mu_p}(k_p r)]$$
$$\sigma_{p3}(k_p, r) = \Re_p[Y_{\mu_p}(k_p r)], \quad \Re_p(\cdot) = \bar{c}_{33}\frac{d}{dr} + \bar{c}_{13}\frac{1}{r} \tag{19}$$

2.2 Solution for functionally graded elastic ring

Consider the elastic ring is made of functionally graded materials (FGMs). Assume the elastic ring is graded as a power-law variation form along the radial direction (Horgan and Chan 1999, Jabbari *et al*. 2002, Abd-alla and Farhan 2008, Khoshgoftar *et al*. 2009)

$$c_{ij}(r) = (r/b)^{2\beta} C_{ij}, \quad \rho(r) = (r/b)^{2\beta} B \tag{20}$$

where β is the material inhomogeneity index, B and C_{ij} are constants.

The governing equations for orthotropic functionally graded (FG) elastic ring under plane stress state can also be obtained by following the similar procedure for piezoelectric ring and are listed here as

$$\frac{d\sigma_{rr}}{dr} + \frac{\sigma_{rr} - \sigma_{\theta\theta}}{r} + B\left(\frac{r}{b}\right)^{2\beta}\omega^2 u_r = 0 \tag{21}$$

$$\sigma_{\theta\theta} = \left(\frac{r}{b}\right)^{2\beta}\left(\tilde{C}_{11}\frac{u_r}{r} + \tilde{C}_{13}\frac{du_r}{dr}\right)$$

$$\sigma_{rr} = \left(\frac{r}{b}\right)^{2\beta}\left(\tilde{C}_{13}\frac{u_r}{r} + \tilde{C}_{33}\frac{du_r}{dr}\right) \tag{22}$$

where

$$\tilde{C}_{11} = C_{11} - \frac{C_{12}^2}{C_{22}}, \quad \tilde{C}_{13} = C_{13} - \frac{C_{12}}{C_{22}}C_{23}, \quad \tilde{C}_{33} = C_{33} - \frac{C_{23}^2}{C_{22}} \tag{23}$$

The substitution of Eq. (22) into Eq. (21) gives

$$\frac{d^2 u_r}{dr^2} + (2\beta + 1)\frac{1}{r}\frac{du_r}{dr} + \left[\frac{B\omega^2}{\tilde{C}_{33}} - \frac{\tilde{C}_{11} - 2\beta\tilde{C}_{13}}{\tilde{C}_{33}}\frac{1}{r^2}\right]u_r = 0 \tag{24}$$

The solution of Eq. (24) is

$$u_r(k_e, r) = (r/b)^{-\beta}[A_4 J_{\mu_e}(k_e r) + A_5 Y_{\mu_e}(k_e r)] \tag{25}$$

where

$$k_e = \frac{\omega}{c_e}, \quad c_e = \sqrt{\frac{\tilde{C}_{33}}{B}}, \quad \mu_e = \sqrt{\frac{\tilde{C}_{11} - 2\beta\tilde{C}_{13}}{\tilde{C}_{33}} + \beta^2} \tag{26}$$

Substituting Eq. (25) into the second equation in Eq. (22), the expression of σ_{rr} in FG elastic ring can be obtained as

$$\sigma_{rr}(k_e, r) = A_4\sigma_{e1}(k_e, r) + A_5\sigma_{e2}(k_e, r) \tag{27}$$

where

$$\sigma_{e1}(k_e, r) = \Re_e[J_{\mu_e}(k_e, r)], \quad \sigma_{e2}(k_e, r) = \Re_e[Y_{\mu_e}(k_e r)]$$
$$\Re_e(\cdot) = (r/b)^{\beta}\left[\tilde{C}_{33}\frac{d}{dr} + (\tilde{C}_{13} - \beta\tilde{C}_{33})\frac{1}{r}\right] \tag{28}$$

3. Resonant and anti-resonant frequencies

Suppose the CPT is traction free at the internal and external surfaces and is electrically shorted at the internal surface of the piezoelectric ring ($\Phi_a = 0$). At the external surface of the piezoelectric ring, the CPT is driven by harmonic electric potential excitation $\Phi_0\exp(\mathbf{j}\omega t)$. As mentioned above, the time dependent factor $\exp(\mathbf{j}\omega t)$ is dropped for the sake of brevity. So the boundary conditions are prescribed mathematically as

$$\sigma_{rr}\big|_{r=a} = 0, \quad \sigma_{rr}\big|_{r=c} = 0$$
$$\Phi\big|_{r=a} = 0, \quad \Phi\big|_{r=b} = \Phi_0 \tag{29}$$

Consider the CPT is perfectly bonded at the interface. That is

$$\|u_r\|_{r=b} = 0, \quad \|\sigma_{rr}\|_{r=b} = 0 \tag{30}$$

where the symbol $\|\cdot\|$ denotes the discontinuity of the corresponding field at the interface.

Utilizing the having obtained solutions of the piezoelectric and FG elastic rings and applying the boundary conditions (29) and interfacial conditions (30), yields

$$K_{ij}A_j = F_i \quad (i, j = 1, 5) \tag{31}$$

vwhere

$$K_{11} = \Phi_1(\omega/c_p, b), \quad K_{12} = \Phi_2(\omega/c_p, b), \quad K_{13} = \Phi_3(\omega/c_p, b)$$
$$K_{14} = 0, \quad K_{15} = 0, \quad K_{21} = \sigma_{p1}(\omega/c_p, a), \quad K_{22} = \sigma_{p2}(\omega/c_p, a)$$
$$K_{23} = \sigma_{p3}(\omega/c_p, a), \quad K_{24} = 0, \quad K_{25} = 0, \quad K_{31} = H(\omega b/c_p)$$
$$K_{32} = J_{\mu_p}(\omega b/c_p), \quad K_{33} = Y_{\mu_p}(\omega b/c_p), \quad K_{34} = -J_{\mu_e}(\omega b/c_e)$$
$$K_{35} = -Y_{\mu_e}(\omega b/c_e), \quad K_{41} = \sigma_{p1}(\omega/c_p, b), \quad K_{42} = \sigma_{p2}(\omega/c_p, b)$$
$$K_{43} = \sigma_{p3}(\omega/c_p, b), \quad K_{44} = -\sigma_{e1}(\omega/c_e, b), \quad K_{45} = -\sigma_{e2}(\omega/c_e, b)$$
$$K_{51} = 0, \quad K_{52} = 0, \quad K_{53} = 0, \quad K_{54} = \sigma_{e1}(\omega/c_e, c), \quad K_{55} = \sigma_{e2}(\omega/c_e, c)$$
$$F_1 = \Phi_0, \quad F_2 = 0, \quad F_3 = 0, \quad F_4 = 0, \quad F_5 = 0 \tag{32}$$

It should be mentioned here that we have four boundary conditions and two continuity conditions, see Eqs. (29) and (30), while only five unknown constants $A_j (j = 1, 5)$ need to be determined. This is because the electric boundary condition at the inner surface is satisfied automatically by using the definite integral for Eq. (8). Ultimately, we have five equations to determine all five unknown constants $A_j (j = 1, 5)$, see Eq. (31).

Consider the homogeneous boundary conditions, i.e., $\Phi_0 = 0$. The existence of nontrivial solution of Eq. (31) leads to

$$\det(K) = 0 \tag{33}$$

Eq. (33) is the characteristic equation from which the resonant frequency $f_r = \omega_r/(2\pi)$ can be obtained. Also, from Eq. (31), the constant A_1 can be determined as

$$A_1 = \frac{\det(\tilde{K})}{\det(K)}\Phi_0 \tag{34}$$

where

$$\tilde{K} = \begin{bmatrix} K_{22} & K_{23} & K_{24} & K_{25} \\ K_{32} & K_{33} & K_{34} & K_{35} \\ K_{42} & K_{43} & K_{44} & K_{45} \\ K_{52} & K_{53} & K_{54} & K_{55} \end{bmatrix} \tag{35}$$

According to the electricity theory, the charge Q, current I and electric displacement D_r obey the following relations

$$Q = 2\pi r l D_r, \quad I = dQ/dt \tag{36}$$

Recall Eq. (7). Clearly, if $A_1 = 0$, we have $D_r = 0$. Subsequently, we have $Q = 0$ and $I = 0$. From Eq. (34), we know that $A_1 = 0$ requires

$$\det(\tilde{K}) = 0 \tag{37}$$

Eq. (37) shows that although the CPTs are driven by the external harmonic electric potential excitation, the current response always keeps zero. This case is known as electric anti-resonant phenomenon (Adelman *et al*. 1975). So essentially, Eq. (37) is the characteristic equations to determine the anti-resonant frequency $f_a = \omega_a/(2\pi)$.

With the obtained resonant and anti-resonant frequencies in hand, another important parameter named as effective electro-mechanical coupling factor k_{eff} for evaluating the vibration performance of the CPT can be determined as

$$k_{eff}^2 = 1 - \left(\frac{f_r}{f_a}\right)^2 \tag{38}$$

4. Numerical results and analysis

To illustrate the dynamics behavior of the cylindrical CPTs specifically, numerical computations are carried out based on the above-mentioned theoretical formula. The piezoelectric material is chosen as PZT4 (Dunn and Taya 1994): $c_{11} = c_{22} = 139.0$ GPa , $c_{12} = 77.8$ GPa, $c_{13} = c_{23} = 74.3$ GPa, $c_{33} = 115.0$ GPa, $e_{31} = e_{32} = -5.2$ C/m^2, $e_{33} = 15.1$ C/m^2, $\in_{33} = 5.62 \times 10^{-9}$ F/m, $\rho = 7.5 \times 10^3$ kg/m^3.

The validation of the presented solution is first evaluated. Setting $\beta = 0$ in Eq. (20), the elastic constants and mass density of the elastic ring then become constant. In other words, the elastic ring is homogeneous. In fact, this case has been studied by Liu and Lin (2009) by means of the equivalent circuit method and experiment method. The comparison of the resonant and anti-resonant frequencies obtained by three different methods is shown in Table 1. In the calculation, we suppose the elastic ring is made of Aluminum: The Young's modulus and poisson ratio are $E = 71.5$ GPa and $\upsilon = 0.34$, respectively and the density is $\rho = 2.7 \times 10^3$ kg/m^3. The inner and outer radii of the piezoelectric ring are fixed at $a = 21$ mm and $b = 26$mm, respectively. Three different values of the thickness of the elastic ring are considered, say $h_e = c - b = 3.9$, 6.5 and 9.1, respectively.

Table 1 shows that the results obtained by three different methods have good agreement. The validity of the present method is thus verified in this respect.

By employing the present solution, the parametric investigations for CPTs will further be demonstrated. In the following analysis, the material parameters for functionally graded elastic ring are adopted as: $C_{11} = C_{22} = C_{33} = 110.05$GPa, $C_{12} = C_{13} = C_{23} = 56.69$ GPa and $B = 2.7 \times 10^3$ kg/m^3.

In the first example, the geometric parameters for PZT4 ring are fixed at $a = 20$ mm and $b = 25$ mm (i.e., the thickness of the piezoelectric ring $h_p = b - a = 5$ mm) while those for the elastic ring are changeable. Figs. 2-4 show the effect of material inhomogeneity index on the fundamental resonant and anti-resonant frequencies, the effective electro-mechanical coupling factor and the fundamental mode shape of the CPTs. Several features can be observed from Fig. 2. (I) For all three values of β, a peak value for both the fundamental resonant and anti-resonant frequencies can be reached with the increase of the thickness of the FG elastic ring (0.5 mm $< h_e <$ 15.0 mm). (II) For $h_e < 9.5$ mm, the fundamental resonant and anti-resonant frequencies increase with the increase of β. While it is contrary for $h_e > 13.0$ mm. (III) The fundamental anti-resonant frequency is always larger than the fundamental resonant frequency. (IV) The inhomogeneity index has little effect on the fundamental resonant and anti-resonant frequencies when the FG elastic ring is thin. But for the CPTs with thick FG elastic ring, the inhomogeneity index has significant effect on the fundamental resonant and anti-resonant frequencies. From Fig. 3, we find that for each β, the effective electro-mechanical coupling factor decrease monotonically with the increase of the thickness of the FG elastic ring. Another important aspect is observed that the effective electro-mechanical coupling factor increases with the decrease of β. For the CPTs with $h_e = 5$ mm, the non-

Table 1 The comparison of the resonant and anti-resonant frequencies obtained by three different methods

h_e (mm)	The present method		The equivalent circuit method (Liu and Lin 2009)		The experiment method (Liu and Lin 2009)	
	f_r (kHz)	f_a (kHz)	f_r (kHz)	f_a (kHz)	f_r (kHz)	f_a (kHz)
3.9	24.132	25.144	24.699	25.284	23.765	24.405
6.5	24.429	25.303	24.952	25.448	24.571	24.943
9.1	24.407	25.173	24.799	25.215	24.453	24.811

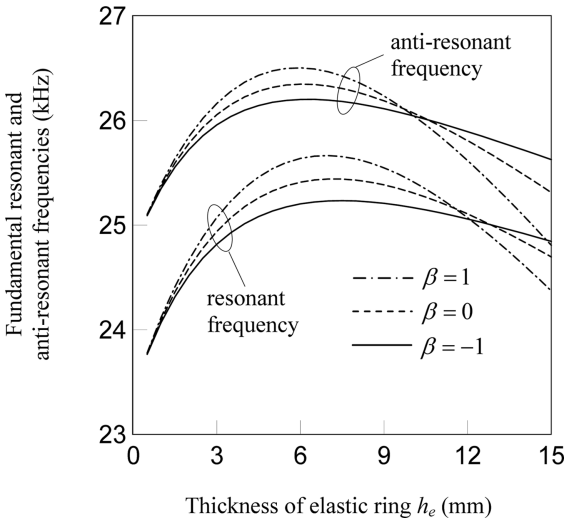

Fig. 2 Fundamental resonant and anti-resonant frequencies versus thickness of the FG elastic ring for different inhomogeneity index

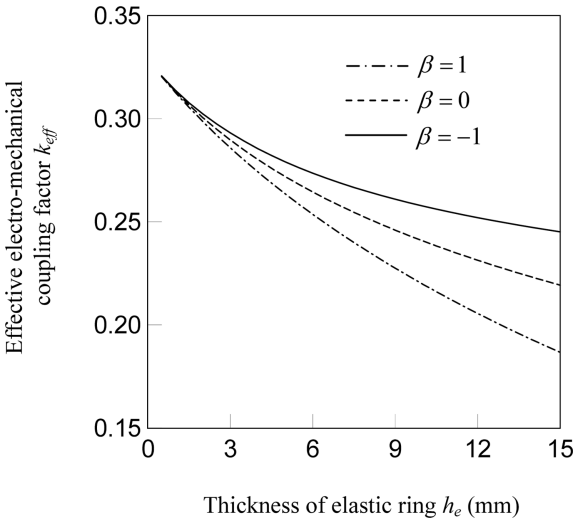

Fig. 3 Effective electro-mechanical coupling factor versus thickness of the FG elastic ring for different inhomogeneity index

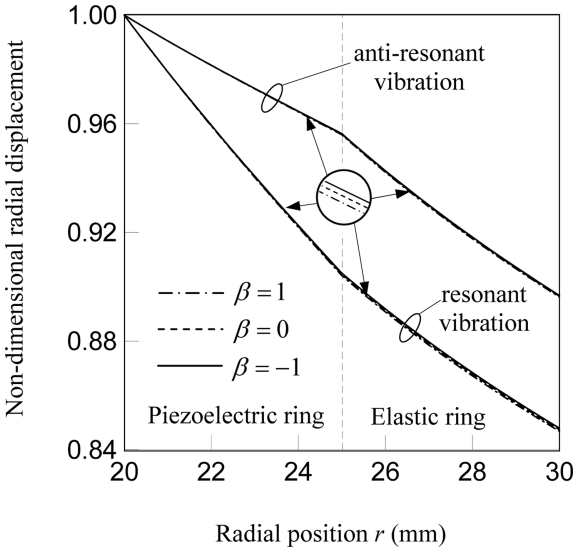

Fig. 4 Fundamental mode shape of CPT for different inhomogeneity index ($h_e = 5$ mm)

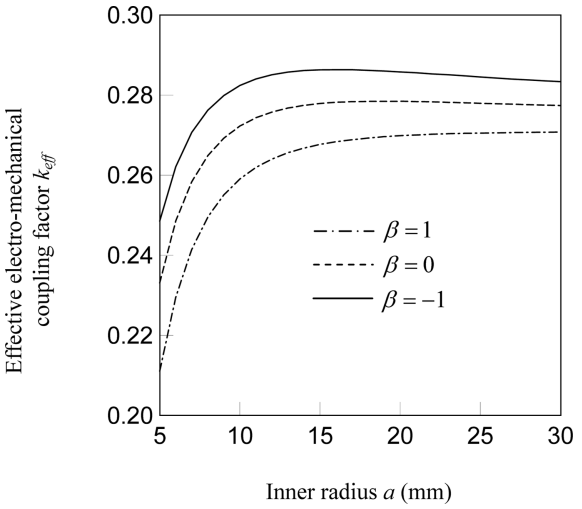

Fig. 5 Effective electro-mechanical coupling factor versus inner radius of the CPTs for different inhomogeneity index

dimensional radial displacements (the radial displacements normalized by the radial displacement at the inner surface) under the excitation with fundamental resonant and anti-resonant frequencies, also named as fundamental mode shape of CPT are depicted in Fig. 4. Clearly, the fundamental mode shape of the CPTs for resonant vibration is different from that for anti-resonant vibration. Also, we can see that the inhomogeneity index β has very little effect on the fundamental mode shape.

Table 2 The fundamental resonant and anti-resonant frequencies of the CPTs integrated with FG elastic ring ($h_p = h_e = 5$ mm)

a (mm)	resonant frequencies (kHz)			anti-resonant frequencies (kHz)		
	$\beta = -1$	$\beta = 0$	$\beta = 1$	$\beta = -1$	$\beta = 0$	$\beta = 1$
5	72.2417	71.3318	69.9320	74.5816	73.3522	71.5440
10	43.8035	43.9039	43.9896	45.6623	45.6277	45.5443
15	31.8138	32.0196	32.2486	33.2041	33.3330	33.4700
20	25.0825	25.2770	25.4930	26.1744	26.3180	26.4753
25	20.7393	20.9054	21.0882	21.6335	21.7632	21.9049
30	17.6931	17.8326	17.9843	18.4494	18.5611	18.6823

In the second example, we consider the dynamic behaviors of the CPTs with different inner radius. To complete this analysis, the thickness of the piezoelectric and elastic rings is set as $h_p = h_e = 5$ mm. Table 2 shows the fundamental resonant and anti-resonant frequencies of the CPTs with different inner radius for $\beta = -1$, 0 and 1. It can be seen that the fundamental resonant and anti-resonant frequencies decrease monotonically with the increase of the inner radius of the CPTs. For small inner radius, e.g., $a = 5$ mm, the fundamental resonant and anti-resonant frequencies decrease with the increase of β. While for large inner radius ($a > 10$ mm), the fundamental resonant and anti-resonant frequencies increase a little bit with the increase of β.

The variation of the effective electro-mechanical coupling factor with the inner radius is depicted in Fig. 5. When the inner radius is small, e.g., $a < 10$ mm, the effective electro-mechanical coupling factor increases with the increase of the inner radius. But when the inner radius is large enough, e.g., $a > 15$ mm, the effective electro-mechanical coupling factor becomes insensitive with the change of the inner radius. Also, we find the effective electro-mechanical coupling factor increase with the decrease of β.

5. Conclusions

The dynamic behaviors of CPTs, such as the fundamental resonant and anti-resonant frequencies, the mode shape as well as effective electro-mechanical coupling factor have been investigated. Numerical results revealed that the material inhomogeneity index and the geometric parameters have important effects on the dynamic behaviors of the CPTs. Based on the above analysis, the following conclusions can be obtained:

(1) Due to acting effect of the inhomogeneity index on the dynamic behaviors, it is an adoptable way to improve the dynamic behaviors of the CPTs by employing the FG elastic ring with proper material inhomogeneity index. Generally speaking, the negative inhomogeneity index is benefit to improve the effective electro-mechanical coupling factor of the CPTs. The inhomogeneity index has little effect on the mode shape.

(2) The effective electro-mechanical coupling factor of the CPTs can be improved by using a large inner radius. While, if we want to increase the fundamental resonant and anti-resonant frequencies, small inner radius will be better.

(3) The presented method can be easily extended to analyze the dynamic behavior of the CPTs with other boundary conditions, such as both the inner and outer surfaces of the CPTs are

mechanical clamped, the inner surface is traction free while the outer surface is mechanical clamped, etc.

In general, the present solution provides a useful methodology to estimate, design and optimize the dynamic behaviors of the CPTs.

Acknowledgements

The work was supported by the National Natural Science Foundation of China (Nos. 10872179, 10725210 and 10832009), the Zhejiang Provincial Natural Science Foundation of China (No. Y7080298), Key Team of Technological Innovation of Zhejiang Province (Grant 2011R09025-05), China Scholarship Council and the Zijin and Xinxing Plans of Zhejiang University.

References

Abd-alla, A.M., Farhan, A.M. (2008), "Effect of the non-homogenity on the composite infinite cylinder of orthotropic material", *Phys. Lett. A,* **372**, 756-760.

Adelman, N.T., Stavsky, Y. and Segal, E. (1975), "Axisymmetric vibrations of radially polarized piezoelectric ceramic cylinders", *J. Sound Vib.*, **38**, 245-254.

Alibeigloo, A. (2009), "Static analysis of a functionally graded cylindrical shell with piezoelectric layers as sensors and actuators", *Smart Mater. Struct.*, **18**, 065004.

Bugdayci, N., Bogy, D.B. and Talke, F.E. (1983), "Axisymmetric motion of radially polarized piezoelectric cylinders used in ink jet printing", *IBM J. Res. Develop.*, **27**, 171-180.

Chen, W.Q., Bian, Z.G., Lv, C.F. and Ding, H.J. (2004), "3D free vibration analysis of a functionally graded piezoelectric hollow cylinder filled with compressible fluid", *Int. J. Solids Struct.*, **41**, 947-964.

Ding, H.J. and Chen, W.Q. (2001), *Three Dimensional Problems of Piezoelasticity*, Nova Science Publishers, New York.

Ding, H.J., Wang, H.M. and Hou, P.F. (2003), "The transient responses of piezoelectric hollow cylinders for axisymmetric plane strain problems", *Int. J. Solids Struct.*, **40**, 105-123.

Dunn, M.L. and Taya, M. (1994), "Electroelastic field concentrations in and around inhomogeneities in piezoelectric solids", *ASME J. Appl. Mech.*, **61**, 474-475.

Elmaimouni, L., Lefebvre, J.E., Ratolojanahary, F.E., Raherison, Gryba T. and Carlier, J. (2011), "Modal analysis and harmonic response of resonators: An extension of a mapped orthogonal functions technique", *Wave Motion*, **48**, 93-104.

Erdelyi, A. (1953), *Higher Transcendental Functions*, McGraw-Hill Book Company, Inc., New York.

Horgan, C.O. and Chan, A.M. (1999), "The pressurized hollow cylinder or disk problem for functionally graded isotropic linearly elastic materials", *J. Elasticity,* **55**, 43-59.

Huang, J.H., Shiah, Y.C. and Lee, B.J. (2008), "Electromechanical responses of a long piezoelectric tube subjected to dynamic loading", *J. Phys. D. Appl. Phys.*, **41**, 025404.

Irschik, H. (2002), "A review on static and dynamic shape control of structures by piezoelectric actuation", *Eng. Struct.*, **24**, 5-11.

Jabbari, M., Sohrabpour, S. and Eslami, M.R. (2002), "Mechanical and thermal stresses in a functionally graded hollow cylinder due to radially symmetric loads", *Int. J. Press. Ves. Pip.*, **79**, 493-497.

Jiang, S.N. and Hu, Y.T. **(**2007), "Analysis of a piezoelectric bimorph plate with a central-attached mass as an energy harvester", *IEEE T. Ultrason. Ferr.,* **54**, 1463-1469.

Khoshgoftar, M.J., Arani, A.G. and Arefi, M. (2009), "Thermoelastic analysis of a thick walled cylinder made of functionally graded piezoelectric material", *Smart Mater. Struct.*, **18**, 115007.

Kim, J.O. and Lee, J.G. (2007), "Dynamic characteristics of piezoelectric cylindrical transducers with radial polarization", *J. Sound Vib.*, **300**, 241-249.

Leinvuo, J.T., Wilson, S.A., Whatmore, R.W. and Cain, M.G. (2007), "A new flextensional piezoelectric ultrasonic motor—Design, fabrication and characterization", *Sensor Actuat. A-Phys.,* **133**, 141-151.
Liu, S.Q. and Lin, S.Y. (2009), "The analysis of the electro-mechanical model of the cylindrical radial composite piezoelectric ceramic transducer", *Sensor Actuat. A-Phys.,* **155**, 175-180.
Lü, C.F., Yang, J.S., Wang, J. and Chen, W.Q. (2009), "Power transmission through a hollow cylinder by acoustic waves and piezoelectric transducers with radial polarization", *J. Sound Vib.*, **325**, 989-999.
Mo, C., Radziemski, L.J. and Clark, W.W. (2010), "Analysis of piezoelectric circular diaphragm energy harvesters for use in a pressure fluctuating system", *Smart Mater. Struct.*, **19**, 025016.
Nye, J.F. (1985), *Physical Properties of Crystals*, Oxford University Press, Oxford.
Ramesh, R. and Ebenezer, D.D. (2005), "Analysis of axially polarized piezoelectric ceramic rings", *Ferroelectrics*, **323**, 17-23.
Rao, M.S. and Narayanan, S. (2007), "Active control of wave propagation in multi-span beams using distributed piezoelectric actuators and sensors", *Smart Mater. Struct.*, **16**, 2577-2594.
Shin, D.Y., Grassia, P. and Derby, B. (2003), "Oscillatory limited compressible fluid flow induced by the radial motion of a thick-walled piezoelectric tube", *J. Acoust. Soc. Am.*, **114**, 1314-1321.
Wang, H.M., Liu, C.B. and Ding, H.J. (2009), "Exact solution for forced torsional vibration of finite piezoelectric hollow cylinder", *Struct. Eng. Mech.*, **31**, 663-678.
Yang, J.S. (2006), *Analysis of Piezoelectric Devices*, World Scientific, Singapore.
Yang, J.S. (2007), "Piezoelectric transformer structural modeling-a review", *IEEE T. Ultrason. Ferr.,* **54**, 1154-1170.
Yu, J.G. and Ma, Q.J. (2008), "Circumferential wave in functionally graded piezoelectric cylindrical curved plates", *Acta Mech.*, **198**, 171-190.
Yu, J.G., Wu, B. and Chen, G.Q. (2009), "Wave characteristics in functionally graded piezoelectric hollow cylinders", *Arch. Appl. Mech.*, **79**, 807-824.
Zhang, T.T., Shi, Z.F. and Spencer, B.F. (2008), "Vibration analysis of a functionally graded piezoelectric cylindrical actuator", *Smart Mater. Struct.*, **17**, 025018.